Coupled mode enhanced giant magnetoplasmonics transverse Kerr effect

L. Halagačka,[1,2*] M. Vanwolleghem,[2,3] K. Postava,[1] B. Dagens,[2] and J. Pištora[1]

[1]*Department of Physics and Nanotechnology Center, Technical University of Ostrava, 17. listopadu 15, 708 33 Ostrava–Poruba, Czech Republic*

[2]*Institut d'Electronique Fondamentale, UMR CNRS 8622, Universite Paris-Sud XI, Orsay, France*

[3]*Institut d'Electronique, Microelectronique et Nanotechnologie, CNRS UMR 8520, Villeneuve-d'Ascq, France*

[*]*lukas.halagacka@gmail.com*

Abstract: We show that the enhancement of the transverse magneto-optical Kerr effect of a smooth magnetic dielectric film covered by a noble metal grating, is strongly dependent on the precise geometry of this grating. Up till now this magnetoplasmonic enhancement was solely attributed to a nonreciprocal shift of the dispersion of the surface plasmon polariton resonances at the interface with the magnetized substrate. It is demonstrated that by hybridization of surface and cavity resonances in this 1D plasmonic grating, the transverse Kerr effect can be further enhanced, extinguished or even switched in sign and that *without* inverting or modifying the film's magnetization. This strong geometrical dispersion and the accompanying anomalous sign change of the magnetoplasmonic effects in such systems has never been considered before, and might find interesting applications in sensing and nanophotonics.

OCIS codes: (250.5403) Plasmonics; (230.3810) Magneto-optic systems; (240.6680) Surface plasmons; (050.6624) Subwavelength structures.

References and links

1. B. Sepulveda, L. Lechuga, and G. Armelles, "Magnetooptic effects in surface-plasmon-polaritons slab waveguides," J. Lightw. Technol. **24**, 945 – 955 (2006).
2. Y. M. Strelniker and D. J. Bergman, "Transmittance and transparency of subwavelength-perforated conducting films in the presence of a magnetic field," Phys. Rev. B **77**, 205113 (2008).
3. V. V. Temnov, G. Armelles, U. Woggon, D. Guzatov, A. Cebollada, A. Garcia-Martin, J.-M. Garcia-Martin, T. Thomay, A. Leitenstorfer, and R. Bratschitsch, "Active magneto-plasmonics in hybrid metalferromagnet structures," Nature Phot. **4**, 107–111 (2010).
4. G. Wurtz, W. Hendren, R. Pollard, R. Atkinson, L. L. Guyader, A. Kirilyuk, T. Rasing, I. I. Smolyaninov, and A. V. Zayats, "Controlling optical transmission through magneto-plasmonic crystals with an external magnetic field," New Journal of Physics **10** (2008).
5. W. Zaets and K. Ando, "Optical waveguide isolator based on nonreciprocal loss/gain amplifier covered by ferromagnetic layer," IEEE Photonics Technol. Lett. **11**, 1012–1014 (1999).
6. M. Vanwolleghem, W. Van Parys, D. Van Thourhout, R. Baets, F. Lelarge, O. Gauthier-Lafaye, B. Thedrez, R. Wirix-Speetjens, and L. Lagae, "Experimental demonstration of nonreciprocal amplified spontaneous emission in a cofe clad semiconductor optical amplifier for use as an integrated optical isolator," Appl. Phys. Lett. **85**, 3980 –3982 (2004).

#190006 - $15.00 USD Received 7 May 2013; revised 12 Jul 2013; accepted 21 Jul 2013; published 9 Sep 2013

7. V. Zayets, H. Saito, S. Yuasa, and K. Ando, "Enhancement of the transverse non-reciprocal magneto-optical effect," Appl. Phys. Lett. **111**, 023103 –023103–7 (2012).
8. V. Temnov, "Ultrafast acousto-magneto-plasmonics," Nature Phot. **6** (2012).
9. G. Ctistis, E. Papaioannou, P. Patoka, J. Gutek, P. Fumagalli, and M. Giersig, "Optical and magnetic properties of hexagonal arrays of subwavelength holes in optically thin cobalt films," Nano Lett. **9**, 1–6 (2009).
10. G. Armelles, A. Cebollada, A. García-Martín, and M. U. González, "Magnetoplasmonics: Combining Magnetic and Plasmonic Functionalities," Advanced Optical Materials **1**, 10–35 (2013).
11. G. Armelles, A. Cebollada, A. García-Martín, J. M. García-Martín, M. U. González, J. B. González-Díaz, E. Ferreiro-Vila, and J. F. Torrado, "Magnetoplasmonic nanostructures: systems supporting both plasmonic and magnetic properties," J. Opt. A: Pure Appl. Opt. **11**, 1464–4258 (2009).
12. V. I. Belotelov, D. A. Bykov, L. L. Doskolovich, A. N. Kalish, and A. K. Zvezdin, "Extraordinary transmission and giant magneto-optical transverse Kerr effect in plasmonic nanostructured films," J. Opt. Soc. Am. B **26**, 1594–1598 (2009).
13. V. Belotelov, I. Akimov, M. Pohl, V. Kotov, S. Kasture, A. Vengurlekar, A. Gopal, D. Yakovlev, A. Zvezdin, and M. Bayer, "Enhanced magneto-optical effect in magnetoplasmonic crystal," Nature Nanotech. **6**, 370–376 (2011).
14. A. K. Zvezdin and V. A. Kotov, "Modern magnetooptics and magnetooptical materials." (Institute of Physics pub., 1997).
15. Collin, F. Pardo, and R. Teissier, "Horizontal and vertical surface resonances in transmission metallic gratings," J. Opt. A: Pure Appl. Opt. **4**, S154–S160 (2002).
16. F. J. Garcia-Vidal, T. W. Ebbesen, and L. Kuipers, "Light passing through subwavelength apertures," Rev. Mod. Phys. **82**, 729–787 (2010).
17. Y. Ding, J. Yoon, M. Javed, S. Song, and R. Magnusson, "Mapping surface-plasmon polaritons and cavity modes in extraordinary optical transmission," Phot. J., IEEE **3**, 365 –374 (2011).
18. F. Marquier, J. Greffet, S. Collin, F. Pardo, and J. Pelouard, "Resonant transmission through a metallic film due to coupled modes," Opt. Express **13**, 70–76 (2005).
19. H. Zhu and C. Jiang, "Nonreciprocal extraordinary optical transmission through subwavelength slits in metallic film," Opt. Lett. **36**, 1308–1310 (2011).
20. I. A. Akimov, V. I. Belotelov, A. V. Scherbakov, and M. Pohl, "Hybrid structures of magnetic semiconductors and plasmonic crystals: a novel concept for magneto-optical devices." J. Opt. Soc. Am. B **29**, A103–A118 (2012).
21. V. I. Belotelov, D. Bykov, L. L. Doskolovich, N. Kalish, V. Kotov, and K. Zvezdin, "Giant magneto-optical orientational effect in plasmonic heterostructures." Opt. Lett. **34**, 398–400 (2009).
22. E. D. Palik, ed., *Handbook of Optical Constants of Solids I, II, III* (Academic Press, 1991).
23. Š. Višňovský, "Optics in magnetic multilayers and nanostructures," (CRC,2006).
24. B. Vertruyen, R. Cloots, J. S. Abell, T. J. Jackson, R. C. da Silva, E. Popova, and N. Keller, "Curie temperature, exchange integrals, and magneto-optical properties in off-stoichiometric bismuth iron garnet epitaxial films," Phys. Rev. B **78**, 094429 (2008).
25. V. Doorman, J.-P. Krumme, and H. Lenz, "Optical and magneto-optical tensor of bismuth-substitated yttrium-iron-garnet film," J. of App. Phys. **68**, 3544–3553 (1990).
26. L. Li, "Reformulation of the Fourier modal method for surface–relief gratings made with anisotropic materials," J. Mod. Opt. **45**, 1313–1334 (1998).
27. L. Li, "Formulation and comparison of two recursive matrix algorithms for modeling layered diffraction gratings," J. Opt. Soc. Am. A **13**, 1024–1035 (1996).
28. L. Li, "Use of Fourier series in the analysis of discontinuous periodic structures," J. Opt. Soc. Am. A **13**, 1870–1876 (1996).
29. S. Collin, F. Pardo, R. Teissier, and J.-L. Pelouard, "Strong discontinuities in the complex photonic band structure of transmission metallic gratings," Phys. Rev. B **63**, 033107 (2001).
30. G. D'Aguanno, N. Mattiucci, M. J. Bloemer, D. de Ceglia, M. A. Vincenti, and A. Alù, "Transmission resonances in plasmonic metallic gratings," J. Opt. Soc. Am. B **28**, 253–264 (2011).
31. A. T. M. A. Rahman, P. Majewski, and K. Vasilev, "Extraordinary optical transmission: coupling of the Wood-Rayleigh anomaly and the Fabry-Pérot resonance," Opt. Lett. **37**, 1742–1744 (2012).
32. J. J. Burke, G. I. Stegeman, and T. Tamir, "Surface-polariton-like waves guided by thin, lossy metal films," Phys. Rev. B **33**, 5186–5201 (1986).
33. R. H. Ritchie, E. T. Arakawa, J. J. Cowan, and R. N. Hamm, "Surface-plasmon resonance effect in grating diffraction," Phys. Rev. Lett. **21**, 1530–1533 (1968).
34. J. Dionne, L. Sweatlock, H. Atwater, and a. Polman, "Plasmon slot waveguides: Towards chip-scale propagation with subwavelength-scale localization," Phys. Rev. B **73**, 1–9 (2006).
35. C. Koechlin, P. Bouchon, F. Pardo, J. Jaeck, X. Lafosse, J. L. Pelouard, and R. Haidar, "Total routing and absorption of photons in dual color plasmonic antennas," Appl. Phys. Lett. **99**, 241104 –241104–3 (2011).
36. K. Postava, J. Pištora, and Š. Višňovský, "Magneto-optical effects in ultrathin structures at transversal magnetization," Czech J. Phys. B **49**, 1185–1204 (1999).

#190006 - $15.00 USD Received 7 May 2013; revised 12 Jul 2013; accepted 21 Jul 2013; published 9 Sep 2013

1. Introduction

Since about half a decade the rich variety of research activities in the field of plasmonics has seen the addition of yet another interesting application, namely magnetoplasmonics. In search of active functionalities in plasmonic circuitry, the use of an external magnetic control field and magneto-optic (MO) effects has been proposed both in surface plasmon waveguide layouts as well as in grating configurations [1, 2] and has been successfully verified experimentally [3, 4]. Moreover the inherent nonreciprocity of magneto-optical ferromagnetic metals has been exploited to obtain ultracompact and integratable optical magnetoplasmonic isolators [5–7]. The main focus of magnetoplasmonic research has been on the enhancement of the magneto-optic response of a MO material via the excitation of surface plasmon polaritons (SPP) [8]. Even though some interesting results have been reported on Kerr effect enhancement in nanoparticles of pure ferromagnetic metals [9, 10], by far the strongest MO Kerr effect enhancements have been seen by combining the SPP resonance of a noble metal with the gyrotropy of a ferromagnetic metal [11].

The most spectacular effect however has been reported by Belotelov et al. [12, 13] where it was predicted and demonstrated that a very strong transverse MO Kerr effect (TMOKE) of the order of 30% is induced by incorporating a nanostructured Au grating on top of a dielectric transparent magnetic iron garnet that is magnetized in plane and parallel to the gold stripes. TMOKE manifests itself as the relative change of the reflected intensity of p-polarized light incident along a plane perpendicular to the magnetization upon reversal of the latter. Magneto-optics textbooks [14] show that TMOKE is only appreciable on lossy magnetic materials, and that for smooth homogeneous ferromagnetic metal films it is only of the order 0.1%. A TMOKE of 30% predicted and measured in a system where the only magnetically active layer is transparent, is therefore a clear demonstration of the enhancement plasmonic resonances can bring about. It was explained how the nonreciprocal splitting of the dispersion of the SPP's guided by the garnet/Au grating interface causes a nonreciprocal shift of the Wood-plasmon resonances in the extraordinary optical transmission (EOT) and reflection spectrum of this structure, and hence is at the origin of the Kerr effect enhancement.

On the other hand, it has been known for some time now, that EOT effects in 1D gratings are governed both by SPP resonances at the grating's interfaces and Fabry-Perot (FP) cavity resonances in its slits, and possibly even by their mutual coupling [15, 16]. The latter hybridization of these resonances is strongly dependent on the precise geometrical parameters of the grating and can greatly influence the efficiency of the EOT effects at play [17, 18]. In EOT gratings on MO substrates [19–21], the role of the FP cavity modes has commonly been neglected in view of the limited interaction that they present with the MO material. As a result the influence on the magnetoplasmonic properties of geometrical dispersion and the resulting resonance hybridization has not been investigated.

It is this paper's goal to prove that contrary to scientific intuition the hybridization of a Au/-garnet magnetoplasmonic grating's SPP and FP resonances has a profound impact on its MO response, in particular its transverse Kerr effect. By varying the geometry of the gold grating, namely its height and its periodicity, we show numerically how the TMOKE of the specular reflected p-wave is drastically impacted, and can be enhanced, extinguished or even inverted. It is proven how this behavior can be entirely understood by a coupling of SPP resonances (of different orders) and a FP cavity resonance and a simple analytical model is proposed.

The paper is organized as follows. After introducing the structure under study and the used numerical models, Section 3 present the dependence of both types of resonances on the grating's geometry. In Section 4 the TMOKE response is analyzed for various grating geometry. Geometrical dispersion of TMOKE will prove that the hybridization of the resonances is at the origin of an anomalous sign change and enhancement of this effect.

#190006 - $15.00 USD Received 7 May 2013; revised 12 Jul 2013; accepted 21 Jul 2013; published 9 Sep 2013

2. Operation principle of transverse magnetoplasmonic grating

2.1. Basic structure and numerical method

Figure 1 shows the typical structure of a magnetoplasmonic TMOKE grating. The one-dimensional (1D) periodic gold grating is deposited on a transversely magnetized magneto-optic dielectric substrate and illuminated by a *p*-polarized beam. In this paper we present more realistic structure with reasonable dispersion of used gold. The transverse character refers to the orientation of the magnetization with respect to the plane of incidence. As the magnetization is assumed to be parallel to the slits, the incidence plane is perpendicular to the latter and only *p*-polarized light can generate SPP's. In this case of the incidence plane perpendicular to the grating slits, we speak about the *planar* diffraction geometry. If the grating slits are not perpendicular to the plane of incidence the diffraction on the grating is *conical* and the parallel component of the wavevector k_y is than defined by the incident wavevector and angle of the grating rotation. As the result the conical diffraction also provides conversion between *s*- and *p*- polarizations which affect possible excitation of SPPs modes. The geometry of the grating is described by the period Λ, the air-slit width r, and the thickness h_1.

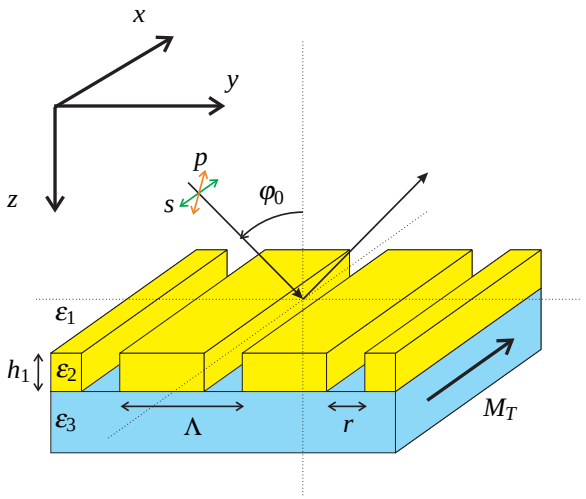

Fig. 1. Coordinate system and schematic representation of studied structure: gold grating with a period Λ and a thickness h_1 on a magneto-optic garnet substrate in transversal configuration with incident plane wave in $y-z$ plane at the incident angle φ_0 and with *s*- or *p*-polarization.

Gold permittivity dispersion is described by a phenomenological Lorentz-Drude model, $\varepsilon_2 = \varepsilon_2(E_{\mathrm{ph}})$, using a Drude term and 2 harmonic Lorentz oscillators terms:

$$\varepsilon_2\left(E_{\mathrm{ph}}\right) = \varepsilon_\infty + \frac{-E_p}{E_{\mathrm{ph}}^2 - \mathrm{i}\Gamma_D E_{\mathrm{ph}}} + \sum_{n=1}^{2} \frac{A_n E_{0,n}^2}{E_{0,n}^2 - E_{\mathrm{ph}}^2 + \mathrm{i}\Gamma_n E_{0,n} E_{\mathrm{ph}}} \tag{1}$$

The plasma energy E_p, the Lorentz resonant frequencies E_n, the damping constants, Γ_D and Γ_n, and the relative oscillator strengths A_n, have been fitted to tabulated data from the Palik handbook in the the spectral range from 0.5 eV to 4.5 eV [22]. For the energy range below 2.2 eV, gold dispersion can be well described by the Drude term. For region above 2.2 eV the interband absorptions of the gold can be fitted by the Lorentz oscillators (DHO). Gold dispersion described by the Drude-Lorentz model or tabulated gold optical functions from measurement

#190006 - $15.00 USD Received 7 May 2013; revised 12 Jul 2013; accepted 21 Jul 2013; published 9 Sep 2013

give possibility to perform simulation in wider spectral range. Fitted parameters are summarized in Table 1.

Table 1. Numerically fitted values of the Lorentz-Drude model Eq. (1).

$\varepsilon_\infty = 3.75$			
Drude	E_p [eV]		Γ_D
	8.24		0.095
DHO	E_0 [eV]	A	Γ
$n=1$	2.87	0.35	0.205
$n=2$	3.97	2.63	0.504

The MO garnet (Bi-substited yttrium iron garnet $Bi_xY_{3-x}Fe_5O_{12}$ or pure BIG, $Bi_3Fe_5O_{12}$) was taken in transversal magneto-optical configuration (i.e. magnetized along the $x-$axis). Up to first order in the magnetization, symmetry arguments and Onsager's principle [23] impose the following form for its permittivity tensor for the magnetization in transverse direction:

$$\hat{\varepsilon}_3 = \begin{bmatrix} \varepsilon_{xx} & 0 & 0 \\ 0 & \varepsilon_{xx} & \varepsilon_{yz} \\ 0 & -\varepsilon_{yz} & \varepsilon_{xx} \end{bmatrix} \tag{2}$$

Since the MO garnet has very low dispersion in the spectral range from 0.5 eV to 1.5 eV (the change of the permittivity is less than 7 %) we have taken $\varepsilon_{xx} = 2.5^2$ without dispersion and $\varepsilon_{yz}(M_T) = \mathrm{i}q(M_T)$, with the gyrotropy $q(M_T^{\mathrm{sat}}) = 0.1$ (at the saturation magnetization M_T^{sat}). The latter being based on an extrapolation of measurement data on Bi:YIG [24,25]. In order to give an idea about the MO strength, this corresponds roughly to a Faraday rotation of $3^\circ/\mu$m. The off-diagonal element ε_{yz} is odd with respect to reverse of magnetization and proportional to the local magnetization, $\varepsilon_{yz}(+M_T) = -\varepsilon_{yz}(-M_T)$. Pure BIG is considered because it is a quasi-transparent dielectric material with record magneto-optical (MO) properties in the visible and infrared parts of the spectrum. Note also that from Eq. (2) it is clear that the *s*- and *p*- polarizations will not couple as long as $\mathbf{k}_{\mathrm{inc}} \perp \mathbf{M}$ and the response of the structure can therefore be modeled for both polarizations separately. In case where $\mathbf{k}_{\mathrm{inc}} \not\perp \mathbf{M}$ or at conical diffraction the MO response of the structure is given by the combination of the transversal and longitudinal MO effect. In such a case conversion between *s*- and *p*- polarizations appears and more advanced analysis of data is needed.

The optical response of the grating has been calculated using own developed software that implements a fully vectorial anisotropic rigorous coupled wave method (RCWA) [26]. The RCWA approach transforms optical field components to finite sum of Fourier harmonics. By this transformation the problem is transformed to eigenvalue problem which can be solved with hight efficiency. For 1D periodic structures the code uses S-matrix formalism [27] and better convergence is achieved by factorization of Fourier series expansion [28]. The result of this analysis is a matrix relationship of the following form:

$$\begin{pmatrix} \mathrm{A}_{\mathrm{up}}^{(1)} \\ \mathrm{A}_{\mathrm{down}}^{(3)} \end{pmatrix} = \mathbf{S}(\omega;k_{\mathrm{y}}) \begin{pmatrix} \mathrm{A}_{\mathrm{up}}^{(3)} \\ \mathrm{A}_{\mathrm{down}}^{(1)} \end{pmatrix} = \begin{pmatrix} \mathbf{T}_{uu}(\omega;k_{\mathrm{y}}) & \mathbf{R}_{ud}(\omega;k_{\mathrm{y}}) \\ \mathbf{R}_{du}(\omega;k_{\mathrm{y}}) & \mathbf{T}_{dd}(\omega;k_{\mathrm{y}}) \end{pmatrix} \begin{pmatrix} \mathrm{A}_{\mathrm{up}}^{(3)} \\ \mathrm{A}_{\mathrm{down}}^{(1)} \end{pmatrix} \tag{3}$$

relating (possible complex) amplitudes of the incoming polarized light from the uniform air superstrate $\left[\mathrm{A}_{\mathrm{down}}^{(1)}\right]$ and substrate $\left[\mathrm{A}_{\mathrm{down}}^{(3)}\right]$ and outgoing (reflected and transmitted) modes $\left[\mathrm{A}_{\mathrm{up}}^{(1)}, \mathrm{A}_{\mathrm{down}}^{(3)}\right]$. Components of the *S*-matrix represents reflection coefficients in the superstrate $\mathbf{R}_{ud}(\omega;k_{\mathrm{y}})$, in the substrate $\mathbf{R}_{du}(\omega;k_{\mathrm{y}})$ and the forward and backward transmission coefficients $\mathbf{T}_{dd}(\omega;k_{\mathrm{y}})$ and $\mathbf{T}_{uu}(\omega;k_{\mathrm{y}})$.

#190006 - $15.00 USD Received 7 May 2013; revised 12 Jul 2013; accepted 21 Jul 2013; published 9 Sep 2013

2.2. *Operation principle*

The transverse MO Kerr effect is usually defined as a the relative change of reflected intensity of *p*-polarized light while the external magnetic field varies its amplitude and orientation [from one saturated state $(+M_T^{\text{sat}})$ to opposite one $(-M_T^{\text{sat}})$]:

$$\delta R_p = \frac{R_p(+M_T) - R_p(-M_T)}{R_p(M_T = 0)}, \tag{4}$$

In our simulations we investigate behavior of the structure under saturated magnetic state ($M_T = M_T^{\text{sat}}$). In this paper we do not normalize the difference of reflected intensity to avoid artificial enhancement of the TMOKE effect than can appear when $R_p(M_T = 0) \to 0$. The TMOKE is then defined as the difference of reflectivity upon magnetization reversal:

$$\Delta R_p = R_p\left(+M_T^{\text{sat}}\right) - R_p\left(-M_T^{\text{sat}}\right). \tag{5}$$

In other words, the presence of the transverse magnetization in the structure breaks Lorentz reciprocity for the *p*-polarized waves (but it does not break the symmetry for the *s*-polarization). The reciprocity of the system depends (among others) on the symmetry of the reflection matrices upon reversal of the tangential component of the incidence wavector, $\mathbf{R}_{ud}^{T}(-k_{\text{inc},y}) = \mathbf{R}_{ud}(k_{\text{inc},y})$. This is equivalent to mirroring the structure of Fig. 1 in a plane perpendicular to the *y*-axis. Even though this is a geometrical symmetry of the system, it is *not* a symmetry of its permittivity profile as $\hat{\varepsilon}_3 \neq \hat{\sigma}_y^{-1}\hat{\varepsilon}_3\hat{\sigma}_y$, with $\hat{\sigma}_y = \begin{pmatrix} 1 & 0 & 0 \\ 0 & -1 & 0 \\ 0 & 0 & 1 \end{pmatrix}$.

A strong TMOKE signature is thus expected for those *p*-polarized grating's resonances that have a pronounced nonreciprocal forward-backward shifting. This is the basic idea behind the plasmonic enhancement of the TMOKE as proposed by Belotelov [12]. As the noble metal/magnetic garnet supports strongly confined *p*-polarized surface waves, these are expected to have a strongly nonreciprocal modal spectrum and therefore a pronounced and enhanced TMOKE response.

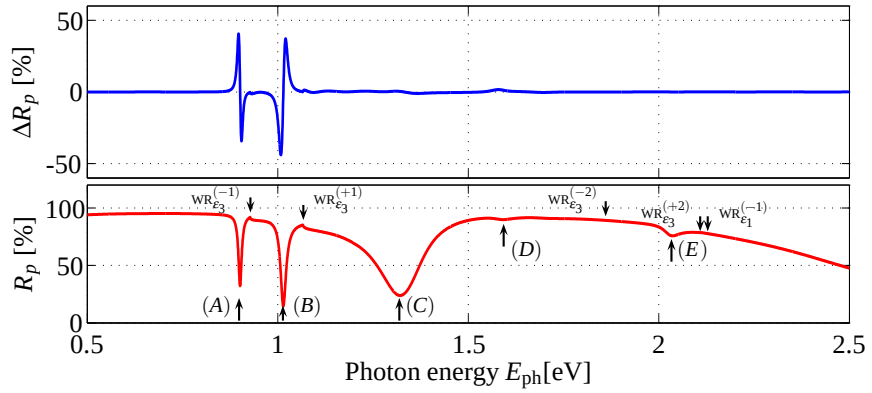

Fig. 2. Specular reflectivity (bottom line) and associated TMOKE spectrum (top line) of p-polarized light incident on the grating structure in Fig. 1 with $\Lambda = 500$ nm, $h_1 = 150$ nm and $r = 20$ nm.

In order to establish the main ideas Fig. 2 shows the specular reflectivity of the structure sample (lower, red curve) and the corresponding TMOKE spectrum (upper, blue curve) for p-polarized light impinging at $\varphi_0 = 10^\circ$ on a typical EOT grating configuration ($\Lambda = 500$ nm, $h_1 = 150$ nm, $r = 20$ nm). One can observe extra-ordinary optical transmission (EOT) resonances as

#190006 - $15.00 USD Received 7 May 2013; revised 12 Jul 2013; accepted 21 Jul 2013; published 9 Sep 2013

pronounced dips in the specular reflection close to 1 eV. It should also be noted that these reflection dips are not related to Wood-Rayleigh (WR) anomalies. The positions of these are given by the crossings of the φ_0-line with the light cones of the sub- and superstrate shifted by multiples of the grating wavenumber, $\frac{2\pi}{\Lambda}$:

$$E_{\text{ph}} = \frac{hc}{\Lambda}\frac{m}{\sqrt{\varepsilon_i} \pm \sin\varphi_0} \qquad i = 1,3, \quad m \in \mathbb{Z}, \tag{6}$$

where m is the diffraction order, and the plus resp. minus sign for the negative resp. positive diffraction orders. The spectral position of the lowest order anomalies are indicated by arrows in Fig. 2 as $\text{WR}_{\varepsilon_i}^{(m)}$. The observed dips in the reflection curve originate therefore from the grating's own resonant modes, or in other words its Bloch modes. Depending on their nature these resonances might experience a more or less important MO response (nonreciprocal spectral shift) upon magnetization reversal, as can be seen from the magnitude of the corresponding TMOKE signature for each EOT resonance (see top subplot in Fig. 2).

Collin has shown how for 1D metallic gratings (excited under a fixed incidence angle) its high $Q-$resonances have in general a SPP character while the Fabry-Perot resonances inside the grating slits have a much lower quality factor [29]. The latter, having a negligible interaction with the MO substrate *and* a low $Q-$factor on top of that, will leave therefore very little trace in the TMOKE spectrum. In Fig. 3 we have plotted field distributions in the grating (in particular $|H_x|^2$) that have been calculated at the different indicated resonances in the EOT spectrum of Fig. 2. This confirms that the high$-Q$ resonances with strong TMOKE effect (A) and (B) are indeed Au/MO substrate SPPs coupled to ± 1 diffraction orders. The proximity of the first order substrate Rayleigh anomalies also reveals their origin. It is also confirmed that (C) is indeed a low Q FP slit resonance. The weaker resonances (D) and (E) close to 1.6eV and 2.1eV are too low in energy to be higher order FP resonances. The first one is suspected to be the minus 2$^{\text{nd}}$ order Au/BIG SPP. It has an extremely low quality factor (as confirmed by intensities of an order in magnitude lower) but experiences a strong enough MO shift to still leave a trace in the TMOKE spectrum. The complete absence of TMOKE for the resonance near 2.1eV and the closeness of $\text{WR}_{\varepsilon_1}^{(-1)}$ leaves little doubt that this is the minus 1$^{\text{st}}$ order Au/air SPP, having hardly any overlap with the magnetic substrate. The field plots corresponding to (D) and (E) confirm these predictions.

3. Geometrical dispersion of the grating's resonances

Having reminded the typical resonances in magnetoplasmonic TMOKE spectra, we now turn our attention to their dispersion, in particular as a function of the geometrical parameters of the grating. The obvious aim is to identify whether or not an (anti-)crossing of the cavity modes and the SPP modes occurs and how it impacts the TMOKE response (this phenomena will be discussed in Section 4). Even though it was argued before that the character of the resonances in an EOT grating can hybridize via coupling [18], the impact of geometrical tuning to enhance the EOT levels has only recently been studied [17, 30, 31]. Of these only d'Aguanno et al. [30] expand considerably on the physics of the coupling of the FP slit resonances with the grating's SPPs and its impact on EOT. Apart from studying a hypothetical free standing Ag grating in air, they moreover study this coupling by tuning the incidence angle rather than the geometry of the grating.

It is among others the aim of this article to show how cavity-plasmon modes coupling occurs in magnetoplasmonic gratings and in particular how it can be tuned geometrically for any angle of incidence. For that purpose we consider the specular reflection spectrum R_p as a function of the grating period Λ and the grating thickness h_1. A strong subwavelength slit ($r = 20$ nm)

#190006 - $15.00 USD Received 7 May 2013; revised 12 Jul 2013; accepted 21 Jul 2013; published 9 Sep 2013

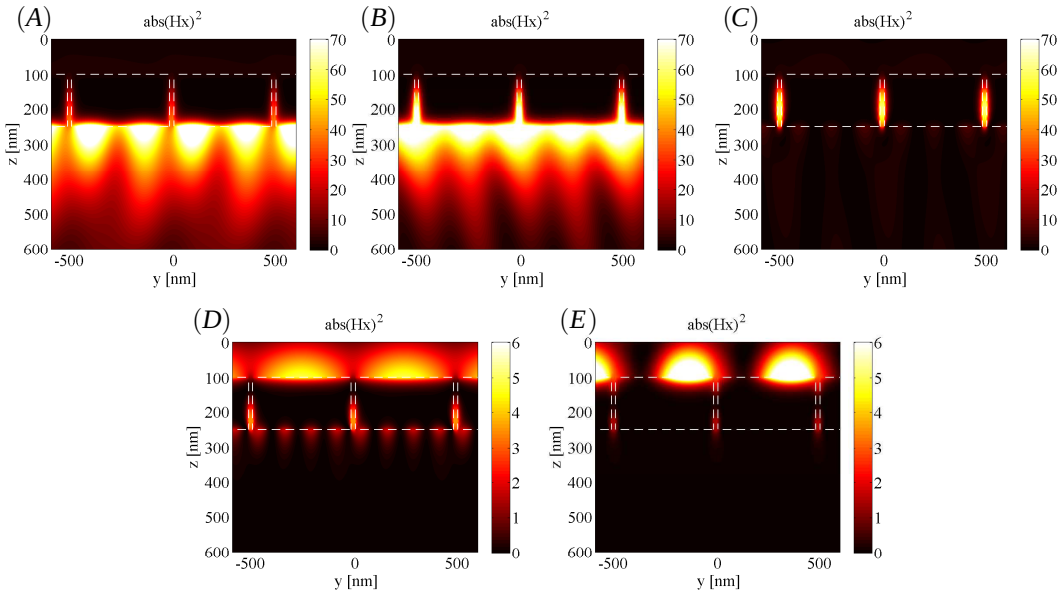

Fig. 3. Distribution of square of the magnitude of the magnetic field component H_x at 0.901 eV (A), at 1.014 eV (B), at 1.318 eV (C), at 1.589 eV (D), at 2.035 eV (E). Field distribution is plotted for grating with the period Λ =500 nm, the thickness $h_1 = 150$ nm, the air-slit width $r = 20$ nm and the incidence of p-polarization at $\varphi_0 = 10^\circ$.

ensures a monomodal regime for the Au/air/Au guide governing the FP resonances. Moreover, as will be shown further down, a small slit ensures low energy fundamental cavity resonances, allowing to study its interaction with plasmon modes for reasonable thicknesses.

3.1. SPP mode dispersion

The loci of the minima in the reflectivity spectrum correspond to the resonant modes in the grating. According to the field plots of Fig. 3 SPPs both on the air/gold and on the gold/garnet interface can be excited. Intuitively, one would assume the plasmon modes to be independent of the grating thickness h_1. Except for sufficiently thin metallic layers (i.e. < 50 nm for near-IR and optical frequencies [32]), the grating interfaces can be considered decoupled and the SPP resonance wavelengths become indeed independent of the grating thickness. The resonances are in good approximation determined by the dispersion relation of the SPP on a single interface:

$$k_{\mathrm{SP}}\left(E_{\mathrm{ph}}\right) = \frac{2\pi}{hc} E_{\mathrm{ph}} \sqrt{\frac{\varepsilon_2\left(E_{\mathrm{ph}}\right)\varepsilon_i}{\varepsilon_2\left(E_{\mathrm{ph}}\right)+\varepsilon_i}}, \qquad i = 1,3, \tag{7}$$

where E_{ph} is the photon energy and $\varepsilon_2(E)$ represents the permittivity of gold described by Eq. (1), $i = 1$ for the SPP on the air/gold and $i = 3$ for the SPP on the gold/garnet interface. In the 1D periodic structure the SPP is excited by the diffracted wave:

$$k_W\left(E_{\mathrm{ph}}\right) = \pm k_{\mathrm{SP}}(E) + m\frac{2\pi}{\Lambda}, \text{ with } m \in \mathbb{Z}, \tag{8}$$

where k_W denotes wavevector of the SPP. This SPP excitation is historically known as a *Wood plasmon*, because it was observed close to Wood-Rayleigh anomalies Eq. (6) [33]. Putting thus

#190006 - $15.00 USD Received 7 May 2013; revised 12 Jul 2013; accepted 21 Jul 2013; published 9 Sep 2013

$k_W = \frac{2\pi}{hc} E_{\mathrm{ph}} \sin\varphi_0$ and solving Eq. (8) for E_{ph} gives us a first order numerical approximation for the height-independent loci of the SPP resonances.

3.2. Cavity mode dispersion

The spectral position of the slit resonances can, with a good accuracy, be predicted by considering the response of an equivalent FP-like slab resonator: a layer with an index n_{eff}, the same thickness as the gold grating and sandwiched between air and the garnet substrate. The effective index n_{eff} is given by the fundamental TM mode of the Au/air/Au guide and it is found as a solution of the dispersion equation [30]:

$$\tanh\left(\frac{r}{2}\sqrt{k_0^2 n_{\mathrm{eff}}^2 - k_0^2}\right) = -\frac{\sqrt{k_0^2 n_{\mathrm{eff}}^2 - k_0^2 \varepsilon_2}}{\varepsilon_2 \sqrt{k_0^2 n_{\mathrm{eff}}^2 - k_0^2}}. \tag{9}$$

The location of the cavity resonances is then found by expressing round-trip resonance:

$$2k_0 n_{\mathrm{eff}} h_1 - \phi_{r_1} + \phi_{r_3} = 2n\pi, \quad n \in \mathbb{Z}, \tag{10}$$

where ϕ_{r_i} is the reflection phase shift of the slit mode at both ends of the cavity. The reflection coefficient can be roughly approximated as a normal-incidence reflection:

$$r_i = |r_i| \exp(\mathrm{i}\phi_{r_i}) = \frac{n_{\mathrm{eff}} - \sqrt{\varepsilon_i}}{n_{\mathrm{eff}} + \sqrt{\varepsilon_i}}, \tag{11}$$

where $i = 1$ for the the permittivity of air and $i = 3$ for the permittivity of the non-magnetized garnet [$\varepsilon_{yz} = 0$ in Eq. (2)]. Such simple approximation is sufficient for cavity mode in regions where it doesn't interact with the plasmon modes. In case of interaction between modes, the reflection phase shift of the mode at both ends of the cavity can be fitted and described in a more precise way [17].

Figure 4 schematically shows the gold/air/gold waveguide and its transformation into resonant cavity. The field plot on the right corresponds to a guide width of 20 nm which is equivalent to the slit width in the grating. At 1.318 eV, i.e. the FP resonance observed in Fig. 2, an effective index of $n_{\mathrm{eff}} = 1.966 + 0.037\mathrm{i}$, is obtained for this mode. As known, this plasmonic slot waveguide has no cut-off for the a_b-mode and this independently of the slit width (see [34]). An extreme subwavelength confinement and accompanying high effective index is therefore obtained at very small slit widths, thereby allowing low energy FP resonances for moderate thicknesses of the metal grating.

3.3. Geometrical dispersion of resonant modes

Analytical description of resonant modes in the structure brings important information about their dependence on the grating's geometry. In summary the dispersion relations Eq. (8,7) and Eq. (9,10) show that the plasmon resonant modes depend on the grating period Λ and the cavity modes depend on the grating thickness h_1 and on the air-slit width $r = f\Lambda$. From Fig. 2 one can see that the TMOKE spectrum achieves its maxima in spectral range from 0.5 eV to 1.5 eV. Therefor we present specular reflectivity spectra $R_p\left(E_{\mathrm{ph}}\right)$ for the various grating thickness h_1 and the grating period Λ in this spectral range.

Figure 5 shows spectral dependence of the specular reflectivity $R_p\left(E_{\mathrm{ph}}\right)$ on grating thickness for a fixed grating period $\Lambda = 500$ nm and an incidence angle of $\varphi_0 = 10^\circ$. In this configuration, the -1^{st} plasmon mode [$m = -1$ in Eq. (7)] is excited at a photon energy of 0.88 eV which is close to the wavelength 1.3 μm commonly used in optical telecommunication. According to

#190006 - $15.00 USD Received 7 May 2013; revised 12 Jul 2013; accepted 21 Jul 2013; published 9 Sep 2013

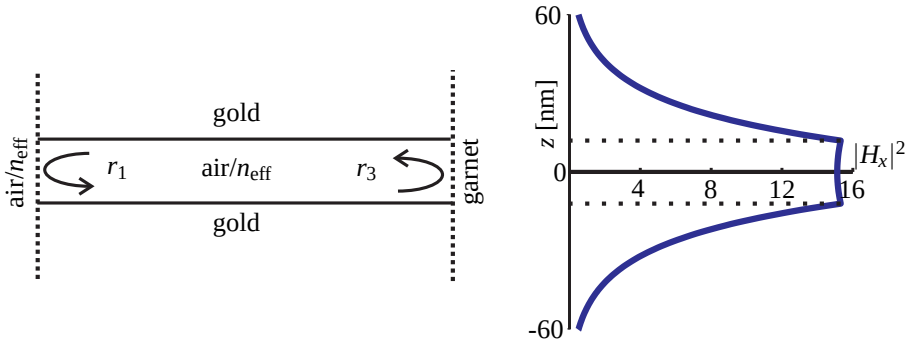

Fig. 4. Left: gold/air/gold waveguide and its extension into resonant cavity by introducing of the garnet and air media is shown schematically. Right: field profile of guided mode for thickness of the air gap $r = 20$ nm, the photon energy 1.318 eV, and the effective index of guided mode $n_{\text{eff}} = 1.966 + 0.0367\text{i}$.

Eq. (8) and Eq. (10) the plasmon modes (blue lines) are dispersion-less under fixed grating period and the cavity modes (red curves) are dispersive respectively. In the left subplot can be seen that the interaction of the cavity modes with the -1^{st} plasmon mode pushes the resonant energy from 1.05 eV (for grating thickness $h_1 = 100$ nm) to 0.91 eV ($h_1 = 330$ nm), which corresponds to smooth transformation between -1^{st} and $+1^{\text{st}}$ plasmon mode. Additional increasing of the grating thickness (up to 330 nm) leads to interaction between the SPP mode and the higher-order cavity modes. Three different orders of the cavity mode correspond to n = 1, 2, and 3 in Eq. (10). Relatively good agreement even from simple approximation is obtained.

Figure 6 shows the spectral dependence of R_p on the grating period Λ in a range of 200 nm to 900 nm and for fixed grating thickness $h_1 = 200$ nm. In this plot the cavity modes are nondispersive for constant thickness h_1 and constant air-slit width $r = \Lambda f = 20$ nm (note that in our model the change of the filling factor f compensates the change of the grating period Λ). On the other hand the plasmon modes show clear dispersive behavior, that is compared with the simple models of Eq. (7) and Eq. (8) on the right subplot. According to Eq. (8) $m = 1$, 2, and, 3 for the plasmon modes at the gold-garnet interface (SPP - ε_3, blue curves), and $m = 1$ for the plasmon at air-gold interface (SPP - ε_1, dashed green curve). The left subplot shows anticrossing behavior of modes. The $\pm 1^{\text{st}}$ horizontal modes and vertical mode are excited separately for a grating period above $\Lambda = 700$ nm. For shorter grating periods (less than 700 nm) anticrossing of modes provides a smooth shift from the -1^{st} plasmon mode ($\Lambda = 700$ nm) to the $+1^{\text{st}}$ mode ($\Lambda = 392$ nm). This is accompanied by a full transformation of the $+1^{\text{st}}$ plasmon mode into the fundamental cavity mode. In addition, the cavity mode at 1.2 eV is more spreaded (wider) for the grating period $\Lambda < 400$ nm. The fill-factor of the air gap is higher (the fill-factor varies with the period) and the Q-factor of the cavity mode is decreased by the interaction of the cavity modes. For longer period the Q-factor of the cavity mode increases due to coupling with hi-Q SPP mode which makes the mode spread narrower.

Note finally, that up to a certain extent periodicity tuning for fixed slit width r and grating height h_1, allows to shift the mode coupling to higher incidence angle. This is of course limited by the SPP gap forming at $E_{\text{ph}} = \frac{hc}{2\Lambda}$ close to which near grazing incidence would be required if the cavity resonance were to be at this energy. A readjustment of the grating thickness is then necessary.

#190006 - $15.00 USD Received 7 May 2013; revised 12 Jul 2013; accepted 21 Jul 2013; published 9 Sep 2013

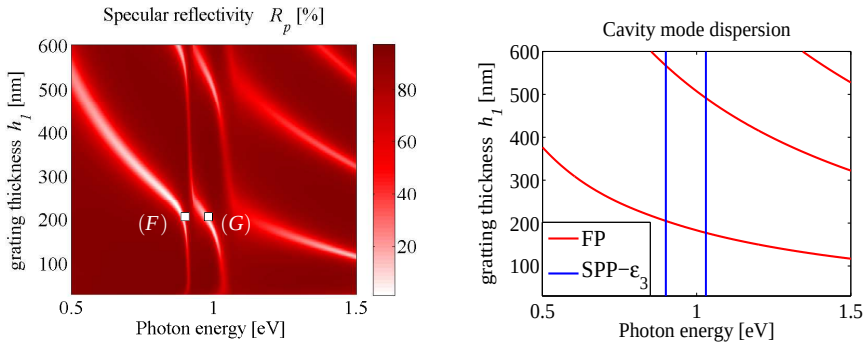

Fig. 5. Left: Simulated dispersion of reflection for the grating with various thickness h_1 from 30 nm to 600 nm and the fixed period $\Lambda = 500$ nm. Right: spectral position and geometrical dispersion of resonant modes calculated with analytical dispersion models Eqs. (8,7) and Eqs. (9,10).

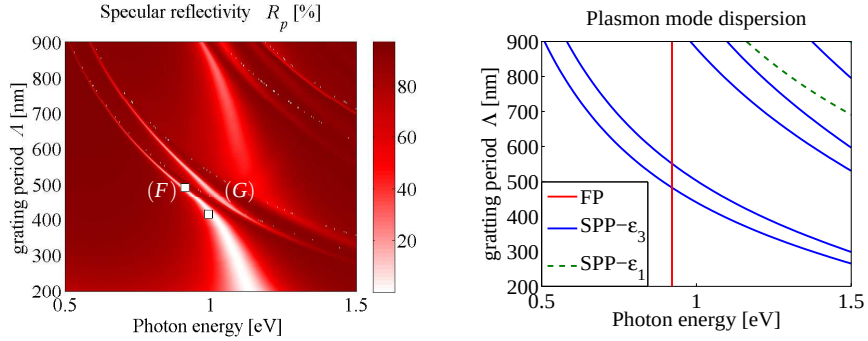

Fig. 6. Left: Simulated dispersion of reflection for the grating with various period Λ from 200 nm to 900 nm and fixed thickness $h_1 = 200$ nm,. Right: spectral position and geometrical dispersion of resonant modes calculated with analytical dispersion models Eq. (8,7) and Eq. (9,10).

3.4. Anticrossing of resonant modes, field plots

Figure 7 shows the field distribution (of the transversal magnetic field component H_x) close to the points of modal anticrossing. Both field distributions were calculated for the grating period $\Lambda = 500$ nm and the modes are marked in the dispersion diagram (Figs. 5, 6). The left subplot shows the field distribution of the $+1^{\text{st}}$ plasmon mode [$m = +1$ in Eq. (8)] coupled with the cavity mode at a photon energy of 0.9 eV and a grating thickness $h_1 = 200$ nm. The right subplot shows field plot of the -1^{st} plasmon mode coupled with the cavity mode at a photon energy of 1 eV and a grating thickness $h_1 = 200$ nm.

From both plots shown on Fig. 7 one can recognize that the field component H_x is much more enhanced than in the case of single resonant mode excitation (Fig. 3, note different color scale). In addition the modes coupling decreases reflection significantly. The reflection is decreased because the excitation of coupled resonant mode increases both absorption [35] *and* the transmission through the sub-wavelength slit aperture. Decrease of reflectivity and strong field enhancement at the interface with MO garnet cause significant increase of the transverse MO effect discussed in the next section.

#190006 - $15.00 USD Received 7 May 2013; revised 12 Jul 2013; accepted 21 Jul 2013; published 9 Sep 2013

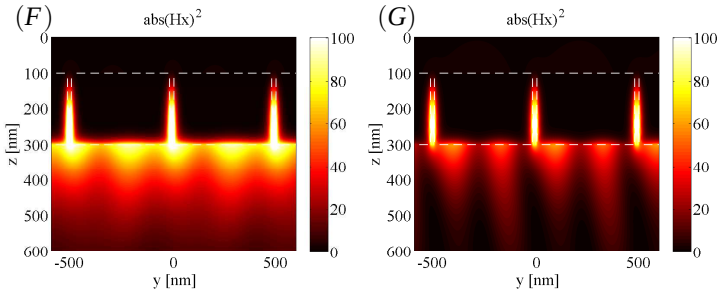

Fig. 7. Distribution of square of the magnitude of the magnetic field component H_x. Left subplot: coupled resonant mode of $+1^{\text{st}}$ plasmon and cavity mode for the photon energy 0.89 eV and the grating thickness 200 nm. Right subplot: coupled resonant mode of -1^{st} plasmon and cavity mode for the photon energy 0.98 eV and the grating thickness 200 nm.

4. Nonreciprocal optical response of grating's resonant modes

Up till now we studied the impact of the grating geometry on the dispersion of its EOT resonances. We now move on to see whether a similar impact can be observed in the nonreciprocal response of this EOT system. In Section 2.2 it was explained how the MO response of this structure can be easily understood at its grating/garnet SPP resonances. In order to describe shift of SPP by transverse magnetooptic Kerr effect we used Yeh's matrix formalism to solve Maxwell's equation for simple interface between metal (gold, ε_2) and dielectric (garnet, ε_3) in transverse MO configuration [Eq. (26-28) in [36]]. Guided mode at the interface (i.e. SPP) is then defined by the resonant condition:

$$\varepsilon_2\left(k_0^2\varepsilon_3-k_{\text{SP}}^2\right)=\left(k_0^2\varepsilon_2-k_{\text{SP}}^2\right)\left(\mathrm{i}qk_{\text{SP}}+\varepsilon_3\sqrt{k_0^2\varepsilon_3-k_{\text{SP}}^2-k_0^2\frac{q^2}{\varepsilon_3}}\right). \tag{12}$$

Considering only linear terms in q, Eq. (12) can be linearized as:

$$k_{\text{SP}}=k_0\left[\sqrt{\frac{\varepsilon_2\varepsilon_3}{\varepsilon_2+\varepsilon_3}}+\frac{\mathrm{i}q\varepsilon_2^2}{\left(\varepsilon_3^2-\varepsilon_2^2\right)\sqrt{\varepsilon_3+\varepsilon_2}}\right], \tag{13}$$

where the first term corresponds to standard surface plasmon resonance Eq. (7) and the second term represents the shift originating from the magneto-optical effect. Our model of the spectral shift of SPP by TMOKE is equivalent with previously used model of SPP shift [13,20]. Figure 8 shows analysis of the shift of SPP calculated (at the photon energy 1 eV) from exact model Eq. (12) and linear approximation Eq. (13) for increased gyrotropy q.

Together with the relation for SPP Eq. (8) it describes phenomena in good agreement with RCWA calculation. Figure 9 shows the shift of the SPP by MO effect. For $q=+0.1$ [and for the MO tensor Eq. (2)] the $+1^{\text{st}}$ SPP mode is shifted to higher energy and vice versa for the -1^{st} SPP. Our linear model of MO-SPP Eq. (13) together with the equation for the Wood plasmon Eq. (8) describes the different shift of $+1^{\text{st}}$ and -1^{st} SPP's resonant frequency. The total wavector shift of the SPP anomalies in the spectra is then given by two contributions: by multiples of wavevector of the grating [Eq. (8)] and by the linear perturbation in Eq. (12).

We have already seen how MO response is obviously related to field confinement in the MO material as shown in Fig. 2 and on the field plots in Fig. 3 (A) and (B). Moreover, the interaction between the plasmon and cavity mode provides strong field enhancement in the MO substrate

#190006 - $15.00 USD Received 7 May 2013; revised 12 Jul 2013; accepted 21 Jul 2013; published 9 Sep 2013

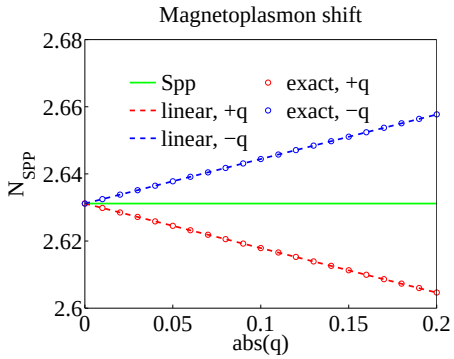

Fig. 8. Shift of SPP by TMOKE: comparison between the exact solution from the Eq. (12) (circle dots) and the linear approximation model Eq. (13) (dashed line) calculated at the photon energy 1eV. The green line represents pure SPP mode.

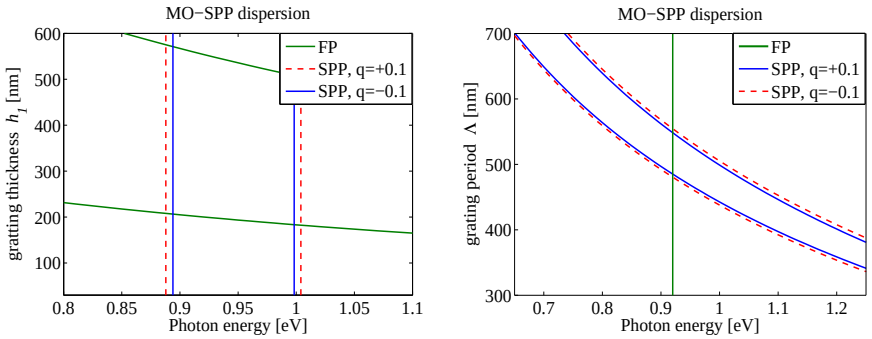

Fig. 9. Magnetooptical shift and dispersion of SPP modes described by Eqs. (12,8) and dispersion curves of cavity modes Eqs. (9,10).

(Fig. 7), which provides a further enhancement of the MO effect. It is therefore expected that in the previously indicated regions of specific modes interaction interesting MO response will appear.

Repeating the same simulations as in Sec. 3.3 we present analysis of the TMOKE spectral dependence on the grating geometry. Figure 10 shows how the TMOKE is affected by interaction between SPP and the cavity modes. Top left subplot shows a detail of the dependence of TMOKE for various grating thicknesses. It is clearly visible that TMOKE of coupled modes keeps the same dispersive dependence as already observed on the specular reflection in non-magneto-optic case (Fig. 5). In addition this suplot shows effective area where coupled mode can exist. In this area the coupled mode has characteristic properties of both SPP and cavity modes. SPP contribution to coupled mode behavior gives MO response and cavity mode contribution gives dependence on the grating thickness.

Top right subplot shows spectral dependence of the TMOKE for chosen thicknesses of the grating. The spectral maximum of the TMOKE varies with the grating thickness and the amplitude changes with the thickness. For the thickness of 170 nm the TMOKE reaches its maximal amplitude (at 0.9 eV). In this point the coupling between modes provides maximal enhancement of the TMOKE. For the thicker or thinner grating the coupling efficiency decreases as well as MO response. Another interesting token of the mode interaction is shown on the bottom left subplot. Since the interaction between modes changes their geometrical dispersion, possible

#190006 - $15.00 USD Received 7 May 2013; revised 12 Jul 2013; accepted 21 Jul 2013; published 9 Sep 2013

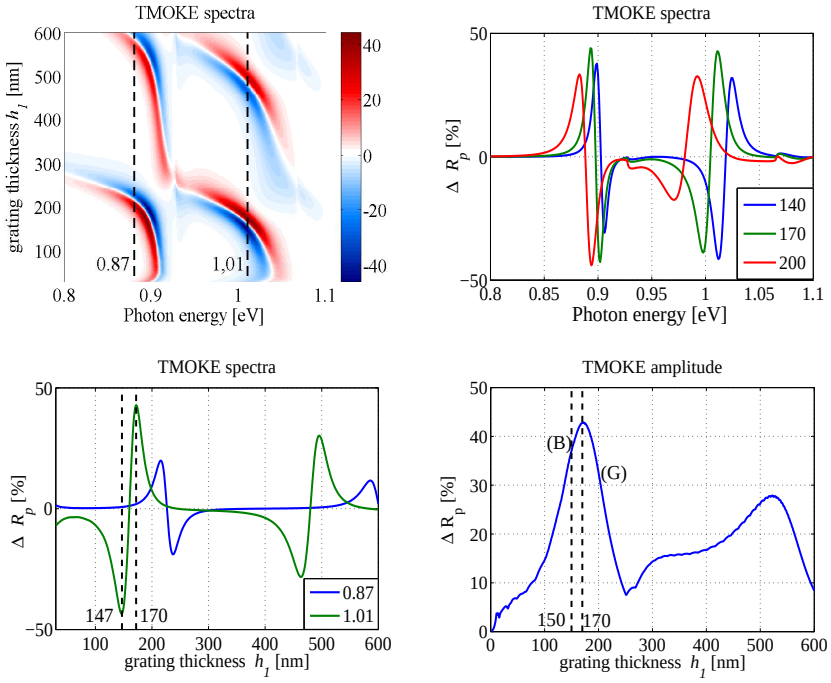

Fig. 10. Top left: detail of TMOKE spectral dependence ΔR_p for the grating thickness h_1 from 30 nm to 600 nm (left) and period $\Lambda = 500$ nm. Top right: variance of the TMOKE spectral position and amplitude for chosen grating thicknesses $h_1 = 140, 170$ and 200 nm. Bottom left: switching of the TMOKE sign at fixed photon energy 0.98 eV and 1.01 eV by variation of the thickness of the grating. Bottom right: dependence of the TMOKE amplitude on the grating thickness.

geometrical tuning of the TMOKE appears. By optimization of the structure to the critical operational point the amplitude and the sign of the TMOKE is strongly affected by geometry, i.e. by the efficiency of the modes coupling. In our case the TMOKE can be completely reversed by changing of the grating thickness from 147 nm to 170 nm. To analyze global TMOKE behavior, we found global maxima of the TMOKE by optimization of the grating thickness and the photon energy. The result is shown on the bottom right subplot. Subplot clearly chows strong dependence of the TMOKE on the thickness of the grating. The position of previously calculated field plots are marked. By analysis of the slope of the curve it is possible to distinguish different areas: below 100 nm and between 300 nm and 450 nm the TMOKE amplitude corresponds to pure SPP mode. Once the modes are coupled the amplitude of the TMOKE increases.

In a second step of the analysis we simulated its spectral response for various grating periods Λ. As expected from simulations shown in Fig. 6, anticrosing between a nondispersive cavity

#190006 - $15.00 USD Received 7 May 2013; revised 12 Jul 2013; accepted 21 Jul 2013; published 9 Sep 2013

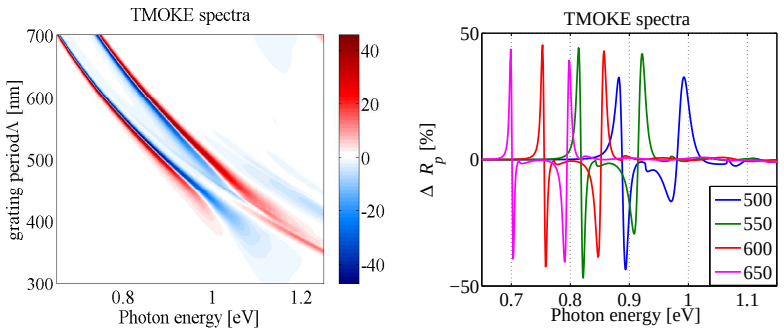

Fig. 11. Left: detail of TMOKE spectral dependence ΔR_p for the grating period Λ from 300 nm to 700 nm (left) and thickness $h_1 = 200$ nm. Right: TMOKE response for chosen grating period $\Lambda = 500,\ 550,\ 600$ and 650 nm.

mode and a dispersive plasmon mode leads to changes in amplitude of the TMOKE. Figure 11 shows on the left subplot the detail of TMOKE spectra for the various grating periods. Obviously the spectral position of the TMOKE peaks changes with the period of the grating but it also changes the amplitude of the TMOKE, which is shown on the right subplot.

5. Conclusion

We have numerically analyzed via a rigorous anisotropic RCWA method the electromagnetic response of a 1D noble metal grating on a transversely magnetized MO substrate. Using straightforward analytical models we have identified geometrical parameter regions where its two basic modes — SPP and FP cavity modes — may potentially couple and interact. By variation of the grating geometry, namely its thickness and period, this interaction and anticrossing has been confirmed. In Sec. 4 it has been shown that this hybridization of SPP and cavity modes leads surprisingly to significant changes in TMOKE amplitude as well as its spectral position. Moreover, the sign of the TMOKE (under fixed magnetization) can be switched by tuning the grating thickness. This sign change can be understood by a transition from a positive to a negative diffractively coupled SPP resonance via hybridization with a FP mode. A linearized model of the MO shift explains the opposite sign s undergone by SPP modes of opposite diffractive coupling. These findings may find interesting applications in new designs for waveguiding structures with a non-reciprocal dispersion of guides modes (e.g. optical isolators for telecommunications) or enhance the efficiency of plasmonic sensors.

Acknowledgment

Partial support from the projects CZ.1.05/1.1.00/02.0070 (IT4Innovations), CZ.1.05/2.1.00/01.0040 (RMTVC), CZ.1.07/2.3.00/20.0074 (Nanobase), Czech Science Foundation 205/11/2137 and SP2013/129 is acknowledged.